STABILISATION OF LOCAL PROJECTION TYPE APPLIED TO CONVECTION-DIFFUSION PROBLEMS WITH MIXED BOUNDARY CONDITIONS*

GUNAR MATTHIES†, PIOTR SKRZYPACZ‡, AND LUTZ TOBISKA‡

Abstract. We present the analysis for the local projection stabilisation applied to convection-diffusion-reaction problems with mixed boundary conditions. We concentrate on the enrichment approach of the local projection methods. Optimal a-priori error estimates will be proved. Numerical tests confirm the theoretical convergence results. Moreover, the local projection stabilisation leads to numerical schemes which work well for problems with several types of layers. Away from layers, the solution is captured very well.

Key words. stabilised finite elements, convection-diffusion-reaction, mixed boundary conditions

AMS subject classifications. 65N12, 65N30, 76D05

1. Introduction. Convection-diffusion-reaction equations occur for instance if physical processes in chemical engineering are modelled. Depending on the problem, different types of boundary conditions are applied on different parts of the domain boundary. A common feature of these problems is the small diffusion coefficient, i.e., the process is convection and/or reaction dominant. Since standard Galerkin discretisations will produce unphysical oscillations for this type of problems, stabilisation techniques have been developed. The streamline-upwind Petrov–Galerkin method (SUPG) has been successfully applied to convection-diffusion-reaction problems. It was proposed by Hughes and Brooks [15]. One fundamental drawback of SUPG is that several terms which include second order derivatives have to be added to the standard Galerkin discretisation in order to ensure consistency. Alternatively, continuous interior penalty methods [1, 6], residual free bubble method [9, 10, 11], or subgrid modelling [8, 14] can be used for stabilising the discretised convection-diffusion-reaction problems.

We will focus in this paper on the local projection stabilisation. This method has been proposed for the Stokes problem in [3]. The extension to the transport problem was given in [4]. The analysis of the local projection method applied to equal-order interpolation discretisation of the Oseen problem can be found in [5, 19]. We will apply the local projection method to convection-diffusion-reaction problems. The stabilisation term of the local projection method is based on a projection $\pi_h : V_h \to D_h$ of the finite element space V_h which approximates the solution into a discontinuous space D_h. The standard Galerkin discretisation is stabilised by adding a term which gives L^2 control over the fluctuation $id - \pi_h$ of the gradient of the solution.

Originally, the local projection technique was proposed as a two-level method where the projection space D_h is defined on a coarser grid. The drawback of this approach is an increased discretisation stencil. The general approach given in [12, 19] allows to construct local projection methods such that the discretisation stencil is not increased compared to the standard Galerkin or the SUPG approach since the

*Partially supported by the German Research Foundation (DFG) through grants To143 and FOR 447.

†Fakultät für Mathematik, Ruhr-Universität Bochum, Universitätsstraße 150, D-44780 Bochum, Germany (Gunar.Matthies@ruhr-uni-bochum.de).

‡Institut für Analysis und Numerik, Otto-von-Guericke-Universität Magdeburg, Postfach 4120, D-39016 Magdeburg, Germany (piotr.skrzypacz,tobiska@mathematik.uni-magdeburg.de).

approximation space Y_h and the projection space D_h are defined on the same mesh. In this case, the approximation space Y_h is enriched compared to standard finite element spaces. We will concentrate in this paper on the enrichment approach of the local projection method.

One objective of this paper is to provide a convergence theory for the local projection method applied to convection-diffusion-reaction problems with mixed boundary conditions. We will prove the same a-priori error estimates which are known for SUPG. Furthermore, several test problems with different types of interior and boundary layers will be presented. They show that the local projection stabilisation allows to obtain numerical solutions which capture the solution away from layers.

The plan of this paper is as follows. Section 2 introduces the considered problem class, the weak formulation, and the local projection stabilisation. An a-priori error estimate for the stabilised discrete problem will be given in Section 3. Numerical results for problems with different type of layers will be presented in Section 4. Conclusions will be given in Section 5.

Notation. The convection-diffusion-reaction problem is considered in a bounded domain $\Omega \subset \mathbb{R}^d$, $d = 2, 3$, with polygonal or polyhedral boundary $\partial\Omega$. For a set D which is either a d-dimensional measurable subset of Ω or a $(d-1)$-dimensional measurable subset of $\partial\Omega$, the Sobolev function spaces $W^{m,p}(D)$ with norm $\|\cdot\|_{m,p,D}$ and seminorm $|\cdot|_{m,p,D}$ are used. As usual, we set $H^m(D) = W^{2,m}(D)$ and skip the index $p = 2$ in the norms and seminorms. The L^2 inner product over $G \subset \Omega$ and $\Gamma \subset \partial\Omega$ will be denoted by $(\cdot,\cdot)_G$ and $\langle\cdot,\cdot\rangle_\Gamma$, respectively. In case $G = \Omega$ the index G will be omitted. For $k \geq 0$ and an d-dimensional subset $G \subset \Omega$, let $P_k(G)$ denote the space of polynomials of degree less than or equal to k while $Q_k(G)$ is the space of all polynomials of degree less than or equal to k in each variable separately.

Throughout this paper, C will denote a generic constant which is independent of the mesh and the diffusion parameter ε. We will use the notation $\alpha \sim \beta$ if there are positive constants C_1 and C_2 such that $C_1\beta \leq \alpha \leq C_2\beta$ holds.

2. Model problem and local projection method.

2.1. Weak formulation. We consider the scalar convection-diffusion-reaction problem with mixed boundary conditions

$$\left.\begin{aligned} -\varepsilon\Delta u + \boldsymbol{b}\cdot\nabla u + cu &= f && \text{in } \Omega,\\ u &= g_D && \text{on } \Gamma_D,\\ \varepsilon\frac{\partial u}{\partial \boldsymbol{n}} &= g_N && \text{on } \Gamma_N, \end{aligned}\right\} \tag{2.1}$$

where $\varepsilon > 0$ is a small constant. The boundary $\partial\Omega$ of Ω consists of two disjoint parts, the Dirichlet part Γ_D and the Neumann part Γ_N. Let Γ_N be a relatively open C^1 part of $\partial\Omega$ and $\Gamma_D = \partial\Omega\setminus\Gamma_N$. The unit outer normal vector with respect to $\partial\Omega$ is denoted by $\boldsymbol{n}$. We are looking for the distribution of concentration u in Ω. The reaction coefficient $c \in L^\infty(\Omega)$ is assumed to be non-negative. Let $f \in L^2(\Omega)$, $g_D \in H^{1/2}(\Gamma_D)$, $g_N \in H^{-1/2}(\Gamma_N)$ be given functions. Furthermore, we require that the convection field $\boldsymbol{b} \in \left(W^{1,\infty}(\Omega)\right)^d$ and the reaction coefficient c fulfil for some $c_0 > 0$ the following condition

$$c(x) - \frac{1}{2}\nabla\cdot\boldsymbol{b}(x) \geq c_0 > 0 \qquad \forall x \in \overline{\Omega}. \tag{2.2}$$

We assume also that the inflow boundary is part of the Dirichlet boundary, i.e.,

$$\left\{x \in \partial\Omega \,:\, (\boldsymbol{b}\cdot\boldsymbol{n})(x) < 0\right\} \subset \Gamma_D. \tag{2.3}$$

We define the function spaces

$$V = H^1(\Omega) \quad \text{and} \quad V_0 = \{v \in V : \ v|_{\Gamma_D} = 0\}.$$

A weak formulation of (2.1) reads

Find $u \in V$ with $u|_{\Gamma_D} = g_D$ such that

$$a(u, v) = (f, v) + \langle g_N, v\rangle_{\Gamma_N} \quad \forall\, v \in V_0 \tag{2.4}$$

where the bilinear form $a : H^1(\Omega) \times H^1(\Omega) \to \mathbb{R}$ is defined by

$$a(u, v) = \varepsilon\,(\nabla u, \nabla v) + (\boldsymbol{b} \cdot \nabla u, v) + (cu, v). \tag{2.5}$$

The conditions (2.2) and (2.3) guarantee the V_0-coercivity of the bilinear form a. The existence and uniqueness of a weak solution of problem (2.4) can be concluded from the Lax–Milgram lemma. For details, we refer to [13].

2.2. Local projection method. For the finite element discretisation of (2.4), we are given a shape regular family $\{\mathcal{T}_h\}$ of decomposition of Ω into d-simplices, quadrilaterals, or hexahedra. The diameter of K will be denoted by h_K and the mesh size parameter h is defined by $h := \max_{K\in\mathcal{T}_h} h_K$. For $\mathcal{T}_h$, let $\mathcal{E}_{h,N}$ denote the set of all edges/faces of cells $K \in \mathcal{T}_h$ which belong to Γ_N.

Let $V_h \subset V$ be a finite element space of continuous, elementwise polynomials of degree $r \geq 1$ over $\mathcal{T}_h$. We fix the polynomial order r and the dependence of constants on r will not be elaborated in this paper. Let

$$V_{0,h} = \{v \in V_h : \ v_h|_{\Gamma_D} = 0\}$$

be the discrete test space.

Since the standard Galerkin discretisation of (2.4) lacks generally stability in the convection dominated regime $\varepsilon \ll 1$, unphysical oscillations will appear in the discrete solution. To circumvent this problem, we consider the stabilisation by the local projection method. Let $D_h(K)$, $K \in \mathcal{T}_h$, be finite dimensional spaces and $\pi_K : L^2(K) \to D_h(K)$ the local L^2 projections into $D_h(K)$. The projection space D_h is given by

$$D_h := \bigoplus_{K\in\mathcal{T}_h} D_h(K).$$

We define the global projection operator $\pi_h : L^2(\Omega) \to D_h$ by $(\pi_h w)|_K = \pi_K(w|_K)$. The fluctuation operator $\kappa_h : L^2(\Omega) \to L^2(\Omega)$ is given by

$$\kappa_h := id - \pi_h$$

where $id : L^2(\Omega) \to L^2(\Omega)$ is the identity mapping in $L^2(\Omega)$. Note that all operators will be applied componentwise to vector-valued functions.

If $P_{r-1}(K) \subset D_h(K)$ holds true for some $r \geq 1$ then we obtain

$$\|\kappa_h q\|_{0,K} \leq C h_K^{\ell} |q|_{\ell,K} \qquad \forall q \in H^{\ell}(K),\, \forall\, 0 \leq \ell \leq r \tag{2.6}$$

by applying the Bramble–Hilbert lemma.

We define the stabilising term

$$S_h(u_h, v_h) := \sum_{K\in\mathcal{T}_h} \tau_K \big(\kappa_h(\nabla u_h), \kappa_h(\nabla v_h)\big)_K \tag{2.7}$$

where τ_K, $K \in \mathcal{T}_h$, denote user-defined parameters. Their choice will be discussed later on. Note that the stabilisation term S_h gives control over the fluctuation of the gradient. An alternative way is to control by

$$\sum_{K\in\mathcal{T}_h} \tau_K \big(\kappa_h(\boldsymbol{b}\cdot\nabla u_h), \kappa_h(\boldsymbol{b}\cdot\nabla v_h)\big)_K$$

only the fluctuation of the derivative in streamline direction.

We can now state the local projection stabilisation of the discretisation of (2.4) as follows

Find $u_h \in V_h$ with $u_h|_{\Gamma_D} = g_{D,h}$ such that

$$a(u_h, v_h) + S_h(u_h, v_h) = (f, v_h) + \langle g_N, v_h\rangle_{\Gamma_N} \quad \forall\, v_h \in V_{0,h} \tag{2.8}$$

where $g_{D,h}$ denotes a suitable approximation of g_D which will be discussed in the next section.

The local projection norm

$$|||v_h||| := \left\{\varepsilon|v_h|_1^2 + c_0\|v_h\|_0^2 + \frac{1}{2}\big\||\boldsymbol{b}\cdot\boldsymbol{n}|^{1/2}v_h\big\|_{0,\Gamma_N}^2 + S_h(v_h, v_h)\right\}^{1/2} \tag{2.9}$$

will be used for our analysis.

The key point in the analysis of local projection method is the existence of an interpolation operator $j_h : H^2(\Omega) \to V_h$ which provides the usual approximation property

$$\|w - j_h w\|_{0,K} + h_K|w - j_h w|_{1,K} \le Ch^\ell \|w\|_{\ell,K} \quad \forall w \in H^\ell(K),\ 2 \le \ell \le r+1 \tag{2.10}$$

and additionally the following orthogonality relation

$$(w - j_h w, q_h) = 0 \quad \forall q_h \in D_h\ \ \forall w \in H^2(\Omega). \tag{2.11}$$

Let

$$Y_h(K) := \big\{w_h|_K\ :\ w_h \in V_{0,h}\,,\ w_h = 0 \text{ on } \Omega\setminus K\big\}$$

denote the local bubble part of the finite element space V_h on K.

A sufficient condition for the existence of an interpolation operator fulfilling (2.10) and (2.11) provides the following lemma.

LEMMA 2.1 (local inf-sup condition). *Let $i_h : H^2(\Omega) \to V_h$ be an interpolation operator which provides for all $K \in \mathcal{T}_h$ the estimate*

$$\|w - i_h w\|_{0,K} + h_K|w - i_h w|_{1,K} \le Ch_K^\ell \|w\|_{\ell,K} \quad \forall w \in H^\ell(K),\ 2 \le \ell \le r+1.$$

Furthermore, let the local inf-sup condition

$$\exists \beta_1 > 0\ \forall h > 0\ \forall K \in \mathcal{T}_h : \inf_{q_h\in D_h(K)} \sup_{v_h\in Y_h(K)} \frac{(v_h, q_h)_K}{\|v_h\|_{0,K}\,\|q_h\|_{0,K}} \ge \beta_1 > 0 \tag{2.12}$$

be satisfied. Then, there exists an interpolation operator $j_h : H^2(\Omega) \to V_h$ possessing the approximation property (2.10) *and the orthogonality property* (2.11).

Proof. For the construction of the interpolation operator j_h, we refer to Theorem 2.2 in [19]. □

In order to satisfy the local inf-sup condition (2.12), the local bubble space $Y_h(K)$ has to be sufficiently large compared to the local projection space $D_h(K)$. However, the minimal dimension of $D_h(K)$ is determined indirectly by (2.6).

Several families of pairs V_h/D_h of approximation spaces V_h and projection spaces D_h which provide the properties (2.10) and (2.11) were given in [19]. We recall here one family on quadrilaterals which was used for our calculation presented in Section 5. Let $F_K : \widehat{K} \to K$ be the multilinear mapping from the reference hypercube $\widehat{K} = (-1, 1)^d$ onto the mesh cell $K \in \mathcal{T}_h$. The projection space D_h is chosen to be the mapped space

$$P_{r-1,h}^{\text{disc}} := \big\{ v \in L^2(\Omega) \,:\, v|_K \circ F_K \in P_{r-1}(\widehat{K}) \;\forall K \in \mathcal{T}_h \big\}.$$

Let

$$\hat{b}(\hat{x}) = \prod_{i=1}^{d} (1 - \hat{x}_i^2), \qquad \hat{x} = (\hat{x}_1, \ldots, \hat{x}_d) \in \widehat{K}$$

be the Q_2 bubble function defined on $\widehat{K}$. The usual local space $Q_r(\widehat{K})$ is enriched to

$$Q_r^{\text{bubble}}(\widehat{K}) := Q_r(\widehat{K}) \oplus \text{span}(\hat{b}\, \hat{x}_i^{r-1} \,,\; i = 1, \ldots, d).$$

The approximation space V_h is set to

$$Q_{r,h}^{\text{bubble}} := \big\{ v \in H^1(\Omega) \,:\, v|_K \circ F_K \in Q_r^{\text{bubble}}(\widehat{K}) \;\forall K \in \mathcal{T}_h \big\}.$$

For $r \geq 1$, the finite element pair $V_h/D_h = Q_{r,h}^{\text{bubble}}/P_{r-1,h}^{\text{disc}}$ satisfies the inf-sup condition (2.12) of Lemma 2.1 and provides the interpolation error estimate from Lemma 2.1. Hence, there exists an interpolation operator j_h satisfying (2.10) and (2.11). For details, see Lemma 4.2 in [19].

Note that we have $P_{r-1}(K) \not\subset P_{r-1,h}^{\text{disc}}(K)$ for non-affine mappings $F_K : \widehat{K} \to K$ but the approximation property (2.6) holds for successively refined meshes, see [2, 17, 18].

3. Error analysis. Let us first discuss the choice of the discrete Dirichlet boundary condition $g_{D,h} \in \{v_h|_{\Gamma_D} \,:\, v_h \in V_h\}$. We use an interpolation of g_D which fits to the interpolation j_h such that $g_{D,h} = (j_h u)|_{\Gamma_D}$ for the solution u of (2.4). This is possible since the restriction of the standard nodal interpolation onto Γ_D depends only on nodal values at Γ_D. For example, $g_{D,h}$ for the $Q_{r,h}^{\text{bubble}}$ discretisation is defined as the $Q_{r,h}$ interpolation of g_D on the boundary Γ_D.

We continue with solvability of the stabilised discrete problem (2.8).

LEMMA 3.1 (Solvability). *The stabilised discrete problem* (2.8) *possesses a unique solution.*

Proof. Since $g_D \in H^{1/2}(\Gamma_D)$ and $g_{D,h} \in \{v_h|_{\Gamma_D} \,:\, v_h \in V_h\}$, we can find some extension $\tilde{g}_{D,h}$ such that $\tilde{g}_{D,h} - u_h \in V_{0,h}$. Indeed, $\tilde{g}_{D,h} = j_h u$ is a possible choice. The key argument for showing the solvability of (2.8) is the proof of the coercivity of the stabilised bilinear form $a + S_h$ with respect to the local projection norm $|||\cdot|||$.

Using the conditions (2.2) and (2.3), we obtain for all test functions $v_h \in V_{0,h}$

$$\begin{aligned} a(v_h, v_h) + S_h(v_h, v_h) \\ &= \varepsilon \left|v_h\right|_1^2 + \frac{1}{2} \int\limits_\Omega \boldsymbol{b} \cdot \nabla v_h^2 \, dx + \int\limits_\Omega c v_h^2 \, dx + S_h(v_h, v_h) \\ &= \varepsilon |v_h|_1^2 + \frac{1}{2} \int\limits_{\Gamma_N} (\boldsymbol{b} \cdot \boldsymbol{n}) \, v_h^2 \, ds + \int\limits_\Omega \left(c - \frac{1}{2} \nabla \cdot \boldsymbol{b} \right) \, v_h^2 \, dx + S_h(v_h, v_h) \\ &\geq \left|\left|\left| v_h \right|\right|\right|^2 . \end{aligned} \tag{3.1}$$

Hence, the existence and uniqueness of the discrete solution can be concluded from the Lax–Milgram lemma. □

We will investigate the consistency error which is caused by adding the stabilising term S_h to the weak formulation.

LEMMA 3.2 (Consistency error). *Let u and u_h be solutions of the problems* (2.4) *and* (2.8)*, respectively. Then, the approximated Galerkin orthogonality*

$$(a + S_h)(u - u_h, w_h) = S_h(u, w_h) \quad \forall w_h \in V_{0,h} \tag{3.2}$$

holds true. Let $\tau_K \sim h_K$ and $u \in H^{r+1}(\Omega)$. Then, the estimate

$$|S_h(u, v_h)| \leq C \left(\sum_{K \in \mathcal{T}} h_K^{2r+1} \|u\|_{r+1,K}^2 \right)^{1/2} \left|\left|\left| v_h \right|\right|\right| \quad \forall v_h \in V_h \tag{3.3}$$

is satisfied.

Proof. The relation (3.2) follows by subtracting (2.4) from (2.8). The Cauchy–Schwarz inequality implies

$$|S_h(u, v_h)| \leq S_h(u, u)^{1/2} \, S_h(v_h, v_h)^{1/2}$$

where the definition (2.7) of S_h was used. It follows from (2.6) and $\tau_K \sim h_K$ that

$$S_h(u, u) = \sum_{K \in \mathcal{T}_h} \tau_K \|\kappa_h(\nabla u)\|_{0,K}^2 \leq C \sum_{K \in \mathcal{T}_h} h_K^{2r+1} \, \|u\|_{r+1,K}^2 .$$

Hence, we have

$$|S_h(u, v_h)| \leq C \left(\sum_{K \in \mathcal{T}_h} h_K^{2r+1} \, \|u\|_{r+1,K}^2 \right)^{1/2} \left|\left|\left| v_h \right|\right|\right|$$

and the second assertion is proved. □

Using the previous results, we are now able to formulate and prove our main convergence result.

THEOREM 3.3 (A-priori error estimate). *Assume $\tau_K \sim h_K$. Let $u \in H^{r+1}(\Omega)$ and $u_h \in V_h$ be the solutions of problems* (2.4) *and* (2.8)*, respectively. Then, the a-priori error estimate*

$$\left|\left|\left| u - u_h \right|\right|\right| \leq C \left(\sum_{K \in \mathcal{T}_h} (\varepsilon + h_K) h_K^{2r} \, \|u\|_{r+1,K}^2 \right)^{1/2} \tag{3.4}$$

holds true.

Proof. First, the triangle inequality implies

$$|||u - u_h||| \leq |||u - j_h u||| + |||j_h u - u_h|||. \tag{3.5}$$

In order to proceed with the estimate of the interpolation error in the local projection norm, we provide some auxiliary results concerning the interpolation error on edges/faces and fluctuation operator. We note the following trace estimate on any edge/face $E \subset \partial K$, $K \in \mathcal{T}_h$,

$$\|v\|_{0,E} \leq C h_K^{1/2} |v|_{1,K} + C h_K^{-1/2} \|v\|_{0,K} \quad \forall v \in H^1(K) \tag{3.6}$$

which gives immediately the local interpolation error estimate

$$\|j_h u - u\|_{0,E} \leq C h_K^{r+1/2} \|u\|_{r+1,K} \tag{3.7}$$

on an edge/face $E \subset \partial K$. Furthermore, one can show for $\boldsymbol{b} \in \big(W^{1,\infty}(K)\big)^d$ the estimate

$$\begin{aligned} \|\kappa_h(\boldsymbol{b} \cdot \nabla v_h)\|_{0,K} &\leq C|\boldsymbol{b}|_{1,\infty,K} \|v_h\|_{0,K} + \|\boldsymbol{b}\|_{0,\infty,K} \|\kappa_h(\nabla v_h)\|_{0,K} \\ &\leq C\big(\|v_h\|_{0,K} + \|\kappa_h(\nabla v_h)\|_{0,K}\big), \end{aligned} \tag{3.8}$$

see the proof of Corollary 2.14 in [19].

Using the interpolation error estimates (2.10) and (3.7), the fact $\boldsymbol{b} \in \big(W^{1,\infty}(\Omega)\big)^d$, and the L^2 stability of the fluctuation operator κ_h, we conclude

$$|||u - j_h u||| \leq C \left(\sum_{K \in \mathcal{T}_h} (\varepsilon + h_K^2 + \tau_K) h_K^{2r} \|u\|_{r+1,K}^2 \right)^{1/2}. \tag{3.9}$$

In order to estimate the second error term on the right hand side of (3.5), we use $u_h|_{\Gamma_D} = \big(j_h u\big)|_{\Gamma_D}$ and the $V_{0,h}$ coercivity proved in Lemma 3.1. We obtain by using relation (3.2) from Lemma 3.2

$$\begin{aligned} |||j_h u - u_h|||^2 &\leq a(j_h u - u_h, w_h) + S_h(j_h u - u_h, w_h) \\ &= a(j_h u - u, w_h) + S_h(u, w_h) + S_h(j_h u - u, w_h) \end{aligned} \tag{3.10}$$

where we set $w_h := j_h u - u_h$ for abbreviation.

We start by estimating the first term on the right hand side of (3.9). Using the the Cauchy–Schwarz inequality, interpolation property (2.10) of j_h and the fact $c \in L^\infty(\Omega)$, it follows that

$$\begin{aligned} &\varepsilon\big(\nabla(j_h u - u), \nabla w_h\big) + \big(c(j_h u - u), w_h\big) \\ &\qquad \leq C \left(\sum_{K \in \mathcal{T}_h} (\varepsilon + h_K^2) h_K^{2r} \, \|u\|_{r+1,K}^2 \right)^{1/2} |||w_h|||. \end{aligned} \tag{3.11}$$

In order to estimate the convective term in the bilinear form a, we integrate by parts and obtain

$$\begin{aligned} \big(\boldsymbol{b} \cdot \nabla(j_h u - u), w_h\big) = &- \big(j_h u - u, \boldsymbol{b} \cdot \nabla w_h\big) - \big(j_h u - u, w_h \, (\nabla \cdot \boldsymbol{b})\big) \\ &+ \big\langle (\boldsymbol{b} \cdot \boldsymbol{n}) \, (j_h u - u), w_h \big\rangle_{\Gamma_N}. \end{aligned} \tag{3.12}$$

The three terms will be estimated separately. Using the orthogonality property (2.11) of the interpolation operator j_h, we get

$$\begin{aligned}\big(j_h u - u, \boldsymbol{b}\cdot\nabla w_h\big) &= \big(j_h u - u, \boldsymbol{b}\cdot\nabla w_h\big) - \big(j_h u - u, \pi_h(\boldsymbol{b}\cdot\nabla w_h)\big)\\ &= \big(j_h u - u, \kappa_h(\boldsymbol{b}\cdot\nabla w_h)\big).\end{aligned}$$

Using (3.8) and the approximation property (2.10), we estimate

$$\begin{aligned}\Big|\big(j_h u - u, \boldsymbol{b}\cdot\nabla w_h\big)\Big| &\le \sum_{K\in\mathcal{T}_h} \|j_h u - u\|_{0,K}\,\|\kappa_h(\boldsymbol{b}\cdot\nabla w_h)\|_{0,K}\\ &\le C\sum_{K\in\mathcal{T}_h} h_K^{r+1}\|u\|_{r+1,K}\big(\|w_h\|_{0,K} + \|\kappa_h(\nabla w_h)\|_{0,K}\big)\\ &\le C\left(\sum_{K\in\mathcal{T}_h} h_K^{2r+2}\,\|u\|_{r+1,K}^2\right)^{1/2}\|w_h\|_0\\ &\quad + C\left(\sum_{K\in\mathcal{T}_h} h_K^{2r+2}\,\tau_K^{-1}\|u\|_{r+1,K}^2\right)^{1/2}\left(\sum_{K\in\mathcal{T}_h}\tau_K\|\kappa_h(\nabla w_h)\|_{0,K}^2\right)^{1/2}\end{aligned}$$

and obtain

$$\Big|\big(j_h u - u, \boldsymbol{b}\cdot\nabla w_h\big)\Big| \le C\left(\sum_{K\in\mathcal{T}_h} h_K^{2r+1}\,\|u\|_{r+1,K}^2\right)^{1/2}|||w_h||| \tag{3.13}$$

where $c_0 > 0$ and the choice $\tau_K \sim h_K$ were exploited.

The second term in (3.12) can be estimated as follows

$$\Big|\big(j_h u - u, w_h\,(\nabla\cdot\boldsymbol{b})\big)\Big| \le C\left(\sum_{K\in\mathcal{T}_h} h_K^{2r+2}\,\|u\|_{r+1,K}^2\right)^{1/2}|||w_h||| \tag{3.14}$$

where the interpolation error estimate (2.10), $\boldsymbol{b}\in\big(W^{1,\infty}(\Omega)\big)^d$, and $c_0 > 0$ were used.

Applying (3.7), the last term in (3.12) can be estimates as

$$\begin{aligned}\big\langle(\boldsymbol{b}\cdot\boldsymbol{n})\,(j_h u - u), w_h\big\rangle_{\Gamma_N} &= \sum_{E\in\mathcal{E}_{h,N}} \big\|\,|\boldsymbol{b}\cdot\boldsymbol{n}|^{1/2}\,(j_h u - u)\big\|_{0,E}\,\big\|\,|\boldsymbol{b}\cdot\boldsymbol{n}|^{1/2}\,w_h\big\|_{0,E}\\ &\le C\left(\sum_{K\in\mathcal{T}_h} h_K^{2r+1}\,\|u\|_{r+1,K}^2\right)^{1/2}|||w_h|||\end{aligned} \tag{3.15}$$

where the shape regularity of $\mathcal{T}_h$ and $\boldsymbol{b}\in\big(W^{1,\infty}(\Omega)\big)^d$ were exploited. Putting together the estimates (3.13), (3.14), and (3.15), we get the bound

$$\Big|\big(\boldsymbol{b}\cdot\nabla(j_h u - u), w_h\big)\Big| \le C\left(\sum_{K\in\mathcal{T}_h} h_K^{2r+1}\,\|u\|_{r+1,K}^2\right)^{1/2}|||w_h||| \tag{3.16}$$

for the convective terms in the bilinear form a. Using (3.11) and (3.16), we conclude that

$$\big|a(j_h u - u, w_h)\big| \le C\left(\sum_{K\in\mathcal{T}_h} (\varepsilon + h_K)\,h_K^{2r}\,\|u\|_{r+1,K}^2\right)^{1/2}|||w_h||| \tag{3.17}$$

holds true.

The second term on the right hand side of (3.10) can be handled by Lemma 3.2. We get

$$\big|S_h(u,w_h)\big| \le C \left(\sum_{K\in\mathcal{T}} h_K^{2r+1} \|u\|_{r+1,K}^2 \right)^{1/2} |||w_h|||. \tag{3.18}$$

To estimate the third term of (3.10), we use the Cauchy–Schwarz inequality, the L^2 stability of the fluctuation operator κ_h, the parameter choice $\tau_K \sim h_K$, and the approximation property (2.10) of the interpolation operator j_h. We obtain

$$\begin{aligned} S_h(j_h u - u, w_h) &\le S_h(j_h u - u, j_h u - u)^{1/2}\, S_h(w_h, w_h)^{1/2} \\ &\le \left\{ \sum_{K\in\mathcal{T}_h} \tau_K \|\kappa_h(\nabla(j_h u - u))\|_{0,K}^2 \right\}^{1/2} |||w_h||| \\ &\le C \left(\sum_{K\in\mathcal{T}_h} h_K^{2r+1} \|u\|_{r+1,K}^2 \right)^{1/2} |||w_h|||. \end{aligned} \tag{3.19}$$

Using (3.10) and the estimates (3.17), (3.18), (3.19), we obtain

$$|||j_h u - u_h||| \le C \left(\sum_{K\in\mathcal{T}_h} (\varepsilon + h_K)\, h_K^{2r} \|u\|_{r+1,K}^2 \right)^{1/2}.$$

Combining this with (3.5) and (3.9) yields the assertion (3.4). □

4. Numerical examples. The section will present some numerical result for the local projection stabilisation applied to convection-diffusion-reaction problem. All numerical calculations were performed with finite element package MooNMD [16].

We consider problems on the unit square $\Omega = (0,1)^2$. Our calculations were carried out on quadrilateral meshes which were obtained by successive regular refinement of an initial coarse grid (level 0) consisting of 4×4 congruent squares. The number of

TABLE 4.1
Total number of degrees of freedom.

level	dofs		
	$Q_{1,h}^{\text{bubble}}$	$Q_{2,h}^{\text{bubble}}$	$Q_{3,h}^{\text{bubble}}$
0	41	113	201
1	145	417	753
2	545	1,601	2,913
3	2,113	6,273	11,457
4	8,321	24,833	45,441
5	33,025	98,817	180,993

degrees of freedom for different enriched finite element spaces are given in Tab. 4.1. It is clearly to see that the number of dofs increases by a factor of about 4 from one mesh level to the next finer one.

Since $\tau_K \sim h_K$, compare Theorem 3.3, the stabilisation parameters are chosen as follows

$$\tau_K := \tau_0\, h_K \qquad \forall K \in \mathcal{T}_h$$

where $\tau_0 > 0$ denotes a constant which will be fixed for each of the test problems presented in this section.

We will investigate in this section the behaviour of the local projection stabilisation applied to problems with different kinds of solutions. The presented examples, except the first one, can be found in [7, 21].

4.1. Smooth solution. We start with a problem which has a smooth solution and check the convergence orders which were predicted by Theorem 3.3. Let

$$\varepsilon = 10^{-7}, \quad \boldsymbol{b} = (2,3)^T, \quad c = 1$$

and

$$\Gamma_N := \big\{(x,y) \in \partial\Omega \,:\, x = 1,\, 0 < y < 1\big\}, \qquad \Gamma_D := \partial\Omega \setminus \Gamma_N.$$

The right hand side f, the Dirichlet boundary condition g_D on Γ_D, and the Neumann boundary condition g_N on Γ_N are chosen such that

$$u(x,y) = \sin(\pi x)\, \sin(\pi y)$$

is the solution of (2.1). Tab. 4.2 shows for the enriched quadrilateral elements of first,

TABLE 4.2
Errors $|||u - u_h|||$ and rates of convergence, $\tau_K = 0.1\, h_K$.

level	error and rate					
	$Q_{1,h}^{\text{bubble}}/P_{0,h}^{\text{disc}}$		$Q_{2,h}^{\text{bubble}}/P_{1,h}^{\text{disc}}$		$Q_{3,h}^{\text{bubble}}/P_{2,h}^{\text{disc}}$	
0	8.634e-2		1.515e-2		1.871e-3	
1	3.206e-2	1.429	2.241e-3	2.757	1.696e-4	3.464
2	1.166e-2	1.459	3.423e-4	2.711	1.506e-5	3.494
3	4.166e-3	1.485	5.632e-5	2.603	1.330e-6	3.501
4	1.477e-3	1.496	9.683e-6	2.540	1.174e-7	3.502
5	5.229e-4	1.499	1.694e-6	2.515	1.037e-8	3.501

second, and third order the error in the local projection norm $|||\cdot|||$ on different levels where $\tau_0 = 0.1$ was used. We see that the predicted convergence order of $r + 1/2$ is achieved in all cases. Moreover, we see that higher order finite elements give much more accurate results with less unknowns.

4.2. Solution with exponential layer. We will study now the behaviour of the local projection stabilisation for a problem with an exponential boundary layer. Let

$$\varepsilon = 10^{-7}, \quad \boldsymbol{b} = (0,2)^T, \quad c = 0$$

and

$$\Gamma_D := \partial\Omega, \qquad \Gamma_N := \emptyset.$$

The right hand side f and the Dirichlet boundary condition g_D are chosen such that

$$u(x,y) = (2x-1)\, \frac{1 - \exp\left(\frac{2(1-y)}{\varepsilon}\right)}{1 - \exp\left(-\frac{2}{\varepsilon}\right)}$$

is the solution of (2.1). Note that the solution u exhibits an exponential boundary layer at $y = 1$. Fig. 4.1 shows for the choice $\tau_0 = 0.1$ the numerical solution which was

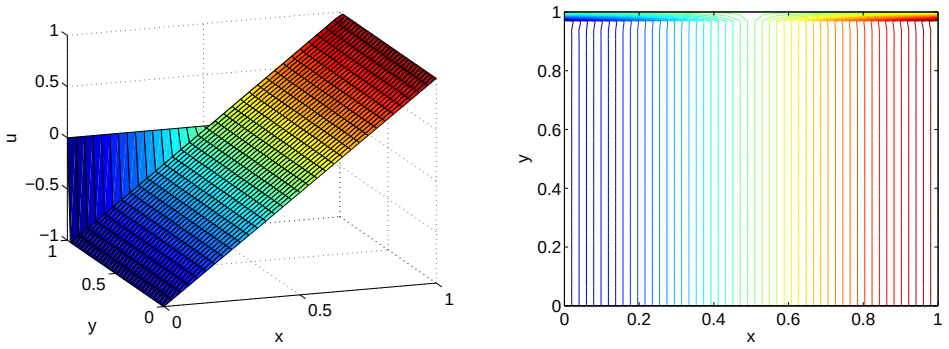

FIG. 4.1. *Example 4.2 with* $V_h/D_h = Q_{1,h}^{bubble}/P_{0,h}^{disc}$ *and* $\tau_0 = 0.1$*: solution (left) and its isolines (right).*

obtained by using the approximation space $Q_{1,h}^{\text{bubble}}$ and the projection space $P_{0,h}^{\text{disc}}$. Note that here and in all subsequent figures only the nodal values at the cell vertices are shown, i.e., the additional bubble part of the solution will not be shown. We see that the numerical solution shows no oscillations in the whole domain. Away from the exponential boundary layer, the numerical solution approximates the function $2x - 1$ which is the solution of the reduced problem.

4.3. Solution with interior and exponential layers. Our next problem is a benchmark for problems with an interior layer and an exponential layer. Let

$$\varepsilon = 10^{-7}, \quad \boldsymbol{b} = \big(8xy(1-x), -4(2x-1)(1-y^2)\big)^T, \qquad c = 0$$

and

$$\Gamma_N := \big\{(x,y) \in \partial\Omega \,:\, 1/2 < x < 1,\, y = 0\big\}, \qquad \Gamma_D := \partial\Omega \setminus \Gamma_N.$$

We prescribe on Dirichlet boundary Γ_D the piecewise constant function

$$g_D(x,y) = \begin{cases} 1 & \text{for } 1/4 \le x \le 1/2\,,\ y = 0, \\ 1 & \text{for } \ 0 \le y \le 1\,,\ x = 1, \\ 0 & \text{otherwise,} \end{cases}$$

while the homogeneous Neumann condition $g_N = 0$ will be used on Γ_N. The right hand side in (2.1) is given by $f = 0$. The numerical solution for $\tau_0 = 0.01$ is presented in Fig. 4.2. It shows overshoots and undershoots near the interior layer and exponential boundary layer. This seems to be a common feature of many stabilisation techniques, see [20]. However, the solution obtained by the local projection stabilisation has no oscillations away from the layer. Furthermore, the position of the layers is captured very well.

4.4. Solution with parabolic layer. The solution of our last example exhibits two parabolic boundary layers. Let

$$\varepsilon = 10^{-7}, \quad \boldsymbol{b} = (0, 1+x^2)^T, \quad c = 0$$

and

$$\Gamma_N := \big\{(x,y) \in \partial\Omega \,:\, 0 < x < 1,\, y = 1\big\}, \qquad \Gamma_D := \partial\Omega \setminus \Omega_N.$$

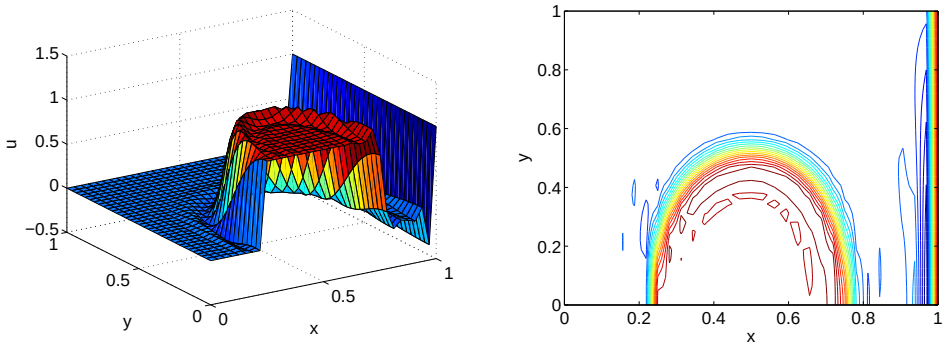

FIG. 4.2. *Example 4.3 with* $V_h/D_h = Q_{1,h}^{bubble}/P_{0,h}^{disc}$ *and* $\tau_0 = 0.01$*: solution (left) and its isolines (right).*

We use homogeneous Neumann condition $g_N = 0$ on Γ_N while the Dirichlet boundary condition g_D on Γ_D is given by

$$g_D = \begin{cases} 1 & \text{for } 0 \le x \le 1,\ y = 0, \\ 1 - y & \text{otherwise.} \end{cases}$$

Furthermore, the right hand side of (2.1) is $f = 0$. Note that the solution of (2.1) exhibits parabolic layers at the vertical walls $x = 0$ and $x = 1$. The pictures in Fig. 4.3

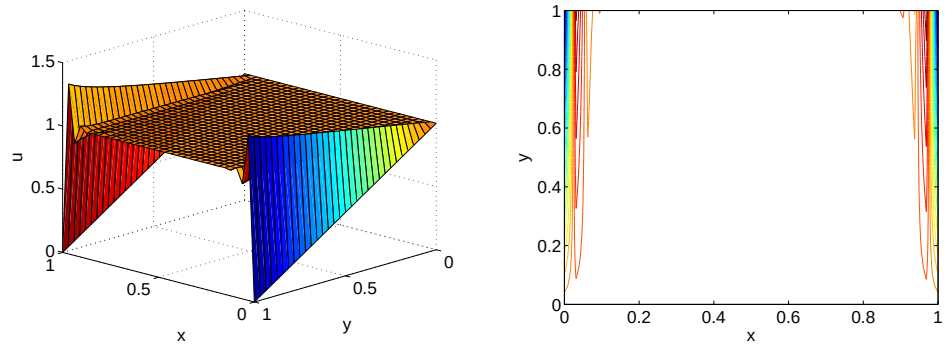

FIG. 4.3. *Example 4.4 with* $V_h/D_h = Q_{1,h}^{bubble}/P_{0,h}^{disc}$ *and* $\tau_0 = 0.01$*: solution (left) and its isolines (right).*

show the obtained result for $\tau_0 = 0.01$. We see that the parabolic boundary layers are well captured. Overshoots and undershoots occur only near the layers while the solution has no oscillations away from the layer.

We are finally interested in the influence of the size of the stabilisation parameter τ_K on the solution. To this end, we will have a look at the solution on the outflow boundary which coincides with Γ_N for this problem. We will vary the constant τ_0 in $\tau_K = \tau_0\, h_K$. We start with calculation for the pair $Q_{1,h}^{\text{bubble}}/P_{0,h}^{\text{disc}}$. The graphs in Fig. 4.4 show that too small values for τ_0 result in oscillations while too large values for τ_0 cause a smearing of the layer. If the constant τ_0 is chosen suitably then the solution is captured very well on almost the whole edge. This means that the remaining small oscillations concentrate near the boundary and only a little smearing takes place.

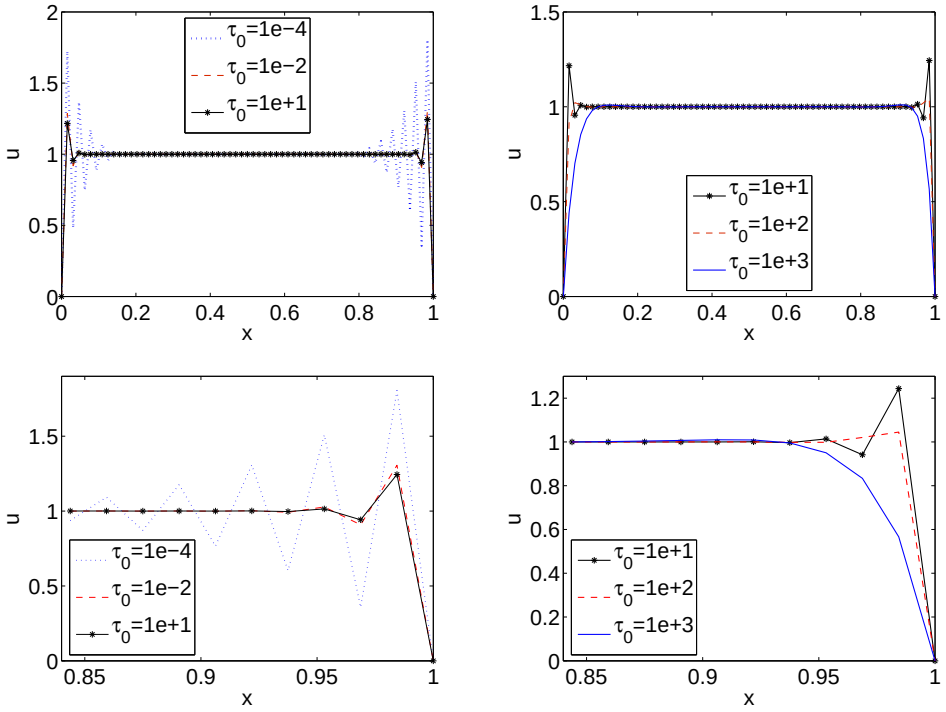

FIG. 4.4. *Example 4.4 with* $V_h/D_h = Q_{1,h}^{bubble}/P_{0,h}^{disc}$*: Influence of parameter* τ_0 *on the behaviour of outflow profile.*

Using the pair $Q_{2,h}^{\text{bubble}}/P_{1,h}^{\text{disc}}$, the situation changes. Even for the quite small stabilisation parameter $\tau_0 = 0.01$, the solution shows no oscillations in the nodal values at the vertices. One reason for this behaviour might be the additional stability

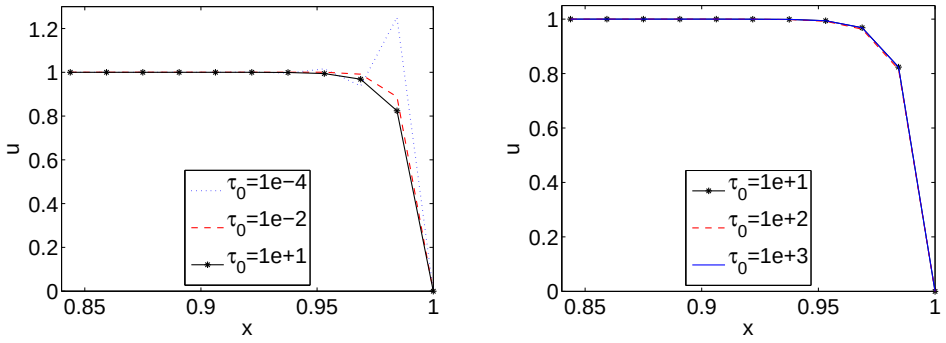

FIG. 4.5. *Example 4.4 with* $V_h/D_h = Q_{2,h}^{bubble}/P_{1,h}^{disc}$*: Influence of parameter* τ_0 *on the behaviour of outflow profile.*

which is already introduced by the presence of bubble functions in $Q_{2,h}^{\text{bubble}}$.

5. Conclusions. We have presented and analysed a stabilised finite element method for solving convection-diffusion-reaction problems. The stabilisation was

achieved by applying the local projection technique which gives additional control over the fluctuation of the gradient. Our analysis handles mixed boundary conditions. The given a-priori error estimate gives qualitatively the same result as other stabilisation techniques like the streamline diffusion method. The numerical results presented in Section 4 show that the stabilisation method by local projection is well suited for problems with layers of different kind. The last example gives the indication that the size of the stabilisation parameter has for first order elements an important influence on the quality of the numerical solution while the dependence is much smaller for second order elements.

REFERENCES

[1] L. E. Alaoui, A. Ern, and E. Burman, *A nonconforming finite element method with face penalty for advection-diffusion equations*, in Numerical mathematics and advanced applications, Springer, Berlin, 2006, pp. 512–519.

[2] D. N. Arnold, D. Boffi, and R. S. Falk, *Approximation by quadrilateral finite elements*, Math. Comp., 71 (2002), pp. 909–922.

[3] R. Becker and M. Braack, *A finite element pressure gradient stabilization for the Stokes equations based on local projections*, Calcolo, 38 (2001), pp. 173–199.

[4] ———, *A two-level stabilization scheme for the Navier-Stokes equations*, in Numerical mathematics and advanced applications, M. Feistauer, V. Dolejší, P. Knobloch, and K. Najzar, eds., Berlin, 2004, Springer-Verlag, pp. 123–130.

[5] M. Braack and E. Burman, *Local projection stabilization for the Oseen problem and its interpretation as a variational multiscale method*, SIAM J. Numer. Anal., 43 (2006), pp. 2544–2566.

[6] E. Burman, *A unified analysis for conforming and nonconforming stabilized finite element methods using interior penalty*, SIAM J. Numer. Anal., 43 (2005), pp. 2012–2033 (electronic).

[7] H. C. Elman, D. J. Silvester, and A. J. Wathen, *Finite elements and fast iterative solvers: with applications in incompressible fluid dynamics*, Numerical Mathematics and Scientific Computation, Oxford University Press, New York, 2005.

[8] A. Ern and J.-L. Guermond, *Theory and practice of finite elements*, vol. 159 of Applied Mathematical Sciences, Springer-Verlag, New York, 2004.

[9] L. P. Franca, *An overview of the residual-free-bubbles method*, in Numerical methods in mechanics (Concepción, 1995), vol. 371 of Pitman Res. Notes Math. Ser., Longman, Harlow, 1997, pp. 83–92.

[10] L. P. Franca and A. Russo, *Deriving upwinding, mass lumping and selective reduced integration by residual-free bubbles*, Appl. Math. Lett., 9 (1996), pp. 83–88.

[11] L. P. Franca and L. Tobiska, *Stability of the residual free bubble method for bilinear finite elements on rectangular grids*, IMA J. Numer. Anal., 22 (2002), pp. 73–87.

[12] S. Ganesan, G. Matthies, and L. Tobiska, *Local projection stabilization of equal order interpolation applied to the Stokes problem*, Preprint 09/2007, Fakultät für Mathematik, Otto-von-Guericke-Universität Magdeburg, 2007.

[13] D. Gilbarg and N. S. Trudinger, *Elliptic partial differential equations of second order*, Classics in Mathematics, Springer-Verlag, Berlin, 2001.

[14] J.-L. Guermond, *Stabilization of Galerkin approximations of transport equations by subgrid modeling*, M2AN, 33 (1999), pp. 1293–1316.

[15] T. J. R. Hughes and A. Brooks, *A multidimensional upwind scheme with no crosswind diffusion*, in Finite element methods for convection dominated flows (Papers, Winter Ann. Meeting Amer. Soc. Mech. Engrs., New York, 1979), vol. 34 of AMD, Amer. Soc. Mech. Engrs. (ASME), New York, 1979, pp. 19–35.

[16] V. John and G. Matthies, *MooNMD—a program package based on mapped finite element methods*, Comput. Vis. Sci., 6 (2004), pp. 163–169.

[17] G. Matthies, *Mapped finite elements on hexahedra. Necessary and sufficient conditions for optimal interpolation errors*, Numer. Algorithm, 27 (2001), pp. 317–327.

[18] G. Matthies and F. Schieweck, *On the reference mapping for quadrilateral and hexahedral finite elements on multilevel adaptive grids*, Computing, 80 (2007), pp. 95–119.

[19] G. Matthies, P. Skrzypacz, and L. Tobiska, *A unified convergence analysis for local projection stabilisations applied to the Oseen problem*, M2AN Math. Model. Numer. Anal., 41

(2007), pp. 713–742.

[20] H.-G. Roos, M. Stynes, and L. Tobiska, *Numerical methods for singularly perturbed differential equations. Convection–diffusion and flow problems*, no. 24 in Springer Series in Computational Mathematics, Springer-Verlag, Berlin, 1996.

[21] Y.-T. Shih and H. C. Elman, *Iterative methods for stabilized discrete convection-diffusion problems*, IMA J. Numer. Anal., 20 (2000), pp. 333–358.